Iron Oxide Nanosized Clusters Embedded in Porous Nanorods: A New Colloidal Design to Enhance Capabilities of MRI Contrast Agents

Aldo F. Rebolledo,[†] Sophie Laurent,[‡] Macarena Calero,[§] Angeles Villanueva,[§] Marcelo Knobel,[⊥] Jose F. Marco,[¶] and Pedro Tartaj[†,*]

[†]Instituto de Ciencia de Materiales de Madrid (CSIC), Campus Universitario de Cantoblanco, 28049, Madrid, Spain, [‡]NMR and Molecular Imaging Laboratory, Department of General, Organic and Biomedical Chemistry, University of Mons-Hainaut, B-7000 Mons, Belgium, [§]Departamento de Biologia, Universidad Autonoma de Madrid, C/Darwin, 2, Cantoblanco, 28049, Madrid, Spain, [⊥]Instituto de Física 'Gleb Wataghin', Universidade Estadual de Campinas CP 6165, 13083-970 Campinas (SP), Brazil, and [¶]Instituto de Química-Física Rocasolano (CSIC), Serrano 119, 28006, Madrid, Spain

T he clinical introduction of nuclear magnetic resonance imaging (MRI) in the early 1980s revolutionized diagnostic imaging. These techniques allow physicians to accurately diagnose pathologies noninvasively. The development of this technique has prompted the need for contrast agents to enhance the image contrast between the normal and diseased tissue and/or to indicate the status of organ functions or blood flow.[1−3] Superparamagnetic compounds were first introduced as contrast agents two decades ago (in the mid-1980s).[4] Nowadays, the present ability to control the size and size distribution of nanoparticles using solution strategies has reignited the search for superparamagnetic contrast agents that have both higher r_2 (transverse relaxivity) and r_2/r_1 values (r_1 is the longitudinal relaxivity) than commercial products ($r_2 = 50−150$ Fe mM^{-1} s^{-1} and $r_2/r_1 = 3−7$). Encapsulation of magnetic nanoparticles in polymeric or organized surfactant assemblies is an approach now routinely used to obtain contrast agents that can have high r_2 and r_2/r_1 values (values of r_2 up to 470 Fe mM^{-1} s^{-1} and $r_1 = 2−3$ Fe mM^{-1} s^{-1} have been reported in magnetic micelles).[5] However, organic matrixes still face unsolved problems, such as their limited chemical and mechanic stability, and swelling (as an alternative an inorganic coating is more stable). Thus, aggregates of MnFe$_2$O$_4$ nanocrystals wrapped first in polymer and then coated with silica−gold nanoparticles can present high relaxivity values ($r_2 = 465$ Fe mM^{-1} s^{-1}).[6] However,

ABSTRACT Development of nanosized materials to enhance the image contrast between the normal and diseased tissue and/or to indicate the status of organ functions or blood flow is essential in nuclear magnetic resonance imaging (MRI). Here we describe a contrast agent based on a new iron oxide design (superparamagnetic iron oxide clusters embedded in antiferromagnetic iron oxide porous nanorods). We show as a proof-of-concept that aqueous colloidal suspensions containing these particles show enhanced-proton relaxivities (*i.e.*, enhanced MRI contrast capabilities). A remarkable feature of this new design is that large scale production is possible since aqueous-based routes are used, and porosity and iron oxide superparamagnetic clusters are directly developed from a single phase. We have also proved with the help of a simple model that the physical basis behind the increase in relaxivities lies on both the increase of dipolar field (interactions within iron oxide clusters) and the decrease of proton-cluster distance (porosity favors the close contact between protons and clusters). Finally, a list of possible steps to follow to enhance capabilities of this contrast agent is also included (partial coating with noble metals to add extra sensing capacity and chemical functionality, to increase the amount of doping while simultaneously carrying out cytotoxicity studies, or to find conditions to further decrease the size of the nanorods and to enhance their stability).

these systems present very low magnetization values (2 emu/g), which for example precludes its use in guiding. Besides, it requires an extensive number of complex steps significantly reducing the production yield of these composites. Another approach to enhance contrast capabilities (search for systems with very high magnetic moment) is the production of well-crystallized hydrophobic nanoparticles using surfactants and high boiling-temperature organic solvents. For example, Zn$_{0.4}$Mn$_{0.6}$Fe$_2$O$_4$ hydrophobic nanoparticles transferred to water using 2,3-dimercaptosuccinic acid (DMSA) present values of r_2 up to 850 Fe mM^{-1} s^{-1} associated with a saturation magnetization of
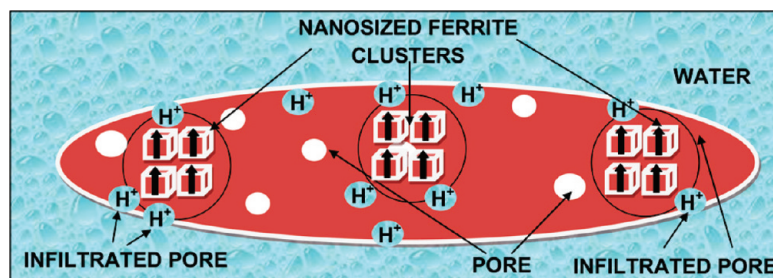
Figure 1. Schematic representation of contrast agents based on a new and simple architectonic design that consists of clusters of ferrite (maghemite) nanoparticles embedded in porous nanorods of hematite. As we will see below the physical basis behind the increase in relaxivities lies on both the increase of dipolar field (interactions within iron oxide clusters) and the decrease of proton-cluster distance (porosity favors the close contact between protons and clusters).

175 emu/g (r_1 values not given).[7] However, this method uses expensive precursors, reactions occur in solution at high temperature, and finally the production yield is low (not in the production of hydrophobic nanoparticles but during the transfer step to aqueous media). Moreover, there is a factor not usually considered; the dipolar interactions scale with the magnetic moment, μ^2, and systems containing nanomagnets with high magnetic moment not embedded or encapsulated in a matrix are highly prompted to timely driven aggregation especially when dealing with the very rich bioenvironments. Therefore, relaxivities are expected to experience a continuous change associated with slight changes in the size of the magnetic aggregates (dipolar interaction scale with the distance, D^3).[8]

From the molecular up to the macroscopic level, the influence of structure on properties is well established (metamaterials are a clear example of entities whose properties mainly stem from their structure).[9] Prompted by our earlier results that it is possible to obtain superparamagnetic nanorods by the controlled thermal reduction of Mn-doped goethite nanorods,[10] we here report the preparation of contrast agents based on a new and simple architectonic design that consists of strongly confined superparamagnetic clusters of maghemite (γ-Fe$_2$O$_3$) nanoparticles embedded in porous colloidal nanorods of slightly canted antiferromagnetic hematite (α-Fe$_2$O$_3$). We show that this colloidal design presents high r_2 and r_2/r_1 values that can be explained by a simple mean field model that takes into consideration interactions within clusters and pore-mediated contact between protons and these clusters. Furthermore, the colloids show an adequate magnetic moment (low enough to significantly increase stability against aggregation but high enough to be guided, if needed, by an external magnetic field). The colloidal design schematically illustrated in Figure 1 possesses remarkable additional features. First, the colloidal composite is purely inorganic and mainly composed of iron oxide (mixture of polymorphs not chemically different components). Second, hydrophilic particles are directly produced with a high production rate and using inorganic salts and water as solvent (in contrast to methods that produce hydrophobic particles). Third, porosity,

γ-Fe$_2$O$_3$ and the rigid α-Fe$_2$O$_3$ matrix are generated from a single iron oxide phase (α-FeOOH, see later). This leads to a system in which the size of the embedded superparamagnetic clusters remains constant, and dipolar interactions are mainly restricted to the clusters within each individual nanorod (as above-mentioned the dipolar interaction scale with the distance, D^3). Thus, we can expect the relaxation of the system to be barely affected by changes in colloidal stability associated with the rich diversity of bioenvironments. Fourthly, despite the superparamagnetic clusters being embedded in a matrix, the porosity of this matrix and its hydrophilic character make possible porous infiltration by the aqueous media, favoring the close contact of protons with the strongly confined superparamagnetic clusters; that is, proton relaxivity is significantly enhanced. Finally, the rod-shape morphology combined with additional monitoring capabilities (say coating with noble metals or semiconductors) may contribute to study the recently established influence of shape in the interaction cell/nanoparticles.[11]

The synthesis route to obtain the iron oxide colloidal nanocomposite is schematically represented in Figure 2 (see Methods for details). Essentially, the experimental methodology is similar to that previously described for the preparation of Mn-doped superparamagnetic nanorods.[10] However, in this work we have extended the methodology by doping with cations such as Ni (II), Cu (II), and Sn (IV) that chemically behave very differently to Mn (II). For example, as we describe in the Methods section, Ni (II) and Cu (II) doped nanorods are sensitive to leaching, and additional treatments are needed. Thus, the method here presented can be, somehow, considered as a generalization. Besides, as we also describe in the Methods section, we have made in this work a better description of the synthesis mechanism in terms of both cation solubility and surface charge density of the solid species present in the system. Briefly, goethite (α-FeOOH) nanorods (80 $\times$ 20 nm) are produced by a carbonate route and subsequently coated with a precursor containing a doping cation (Ni^{2+}, Cu^{2+}, Sn^{4+}) and an alumina external layer. Our approach to efficiently deposit the cation and alumina onto the surface of the nanorods follows a model
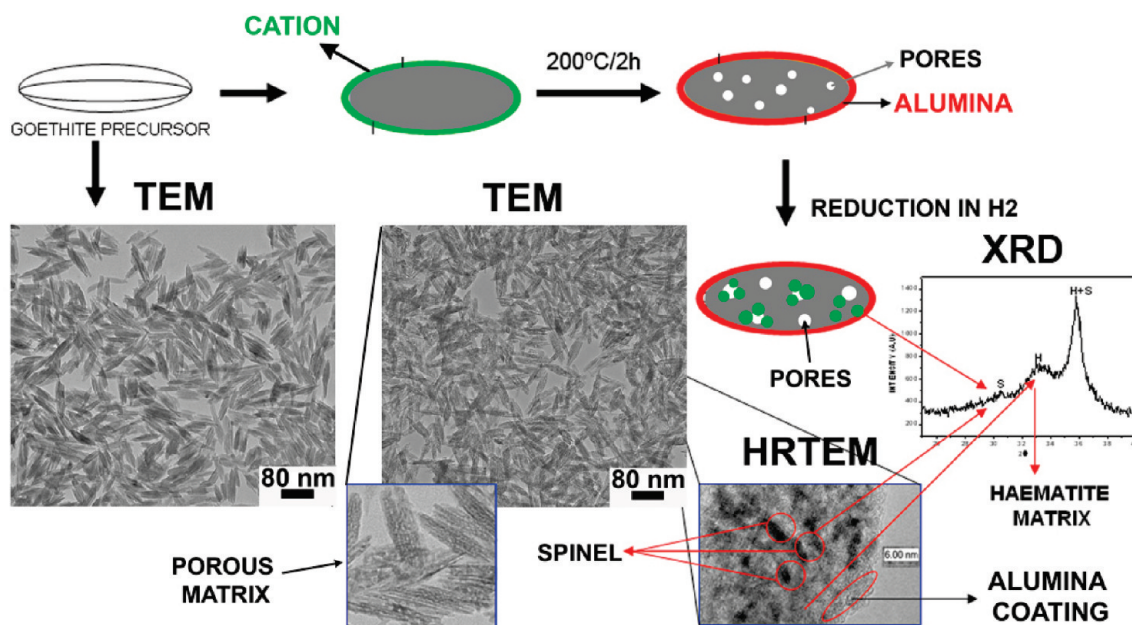
Figure 2. Schematic representation of the process carried out to obtain superparamagnetic maghemite clusters embedded in porous hematite nanorods (see Experimental section in the Supporting Information for details). Uniform goethite nanorods are first obtained and then efficiently coated with a precursor containing the cation of interest. After moderate thermal treatment an alumina layer is deposited. Finally samples are thermally treated in H_2 to develop the spinel phase within the hematite porous nanorods. TEM pictures show the rod-shape morphology of the goethite precursors and the formation of superparamagnetic porous nanorods. EDX chemical analysis carried out on single particle shows similar composition to the bulk assuring homogeneous coatings. X-ray diffraction (XRD) patterns show the presence of diffraction peaks associated with hematite (H in the XRD) and iron oxide spinel (S in the XRD). HRTEM unequivocally indicates domains of spinel encapsulated within the hematite matrix. More detailed information of the content in iron oxide phases can be found in the part of the text dedicated to Mössbauer spectroscopy. Finally, for relaxivity applications the alumina layer was dissolved in basic media to leave the porosity of the matrix available for aqueous infiltration.

that combines the electrostatically driven adsorption induced by cationic or anionic polyelectrolytes (typically used in layer-by-layer electrostatic approaches)[12] with the widely known capabilities of iron oxides to specifically adsorb cationic species in geological environments.[13] Porosity in the hematite matrix is developed as a natural consequence of α-FeOOH dehydroxylation. Alumina avoids interparticle sintering during the thermal reduction treatment needed to develop the maghemite phase. Finally, alumina is dissolved in basic media to leave the porous matrix accessible for aqueous infiltration. Ni (II) and Cu (II) cations were selected as doping cations since they are expected to favor the formation of spinels that display superparamagnetic behavior at room temperature.[14,15] Even though the isomorphous substitution of Fe cations by Sn^{4+} cations in the spinel is not expected to take place, we have selected this cation because we have a very powerful tool to monitor its presence (^{119}Sn Mössbauer). Although the Sn^{4+} ion itself is nonmagnetic, its nucleus can sense a magnetic hyperfine field by supertransferred hyperfine interaction with Fe cations. In this situation the ^{119}Sn Mössbauer spectrum would be expected to be dominated by a single sextet.[16] As we will show below, convincing conclusions about the location of the doping cations can be drawn through the combined characterization of samples with ^{57}Fe and ^{119}Sn Mössbauer spectroscopies. As above-mentioned ferrites doped

with Zn^{2+} produce hydrophobic nanoparticles with a superior magnetic moment and r_2 values.[7] In our case, we have decided not to use Zn (II) because of its high solubility at both acidic and basic pH. Doping with Co (II) was also discarded because this cation makes nanosized ferrites magnetically harder (superparamagnetic effect is not favored).[17] Doping was in all cases restricted to very low values (10 mol %) to make the porosity of the matrix highly available to protons in case the cation was not dissolved within the hematite and/or spinel crystalline structure (as we will show later it turned out to be the case). In addition, limiting the doping concentration to these values assures a system highly enriched in biocompatible iron oxide. Alumina coatings were optimized to a value of 20 wt % with the aim to preserve the rod shape at the highest reduction temperature possible while still displaying no remanence (zero coercivity) in the magnetization curves (as the aforementioned alumina was removed at basic pH after heating). Under these conditions, reduction temperatures were optimized to 275 °C for Sn and Ni-doped samples and only 175 °C for the Cu-doped samples.

Mössbauer spectroscopy provides very useful information about the nature and composition of iron oxide phases present in the samples. At room temperature (RT) the ^{57}Fe Mössbauer spectra of all samples (Figure 3 and Table S1 in Supporting Information for full data) show very broad, asymmetric lines indicating
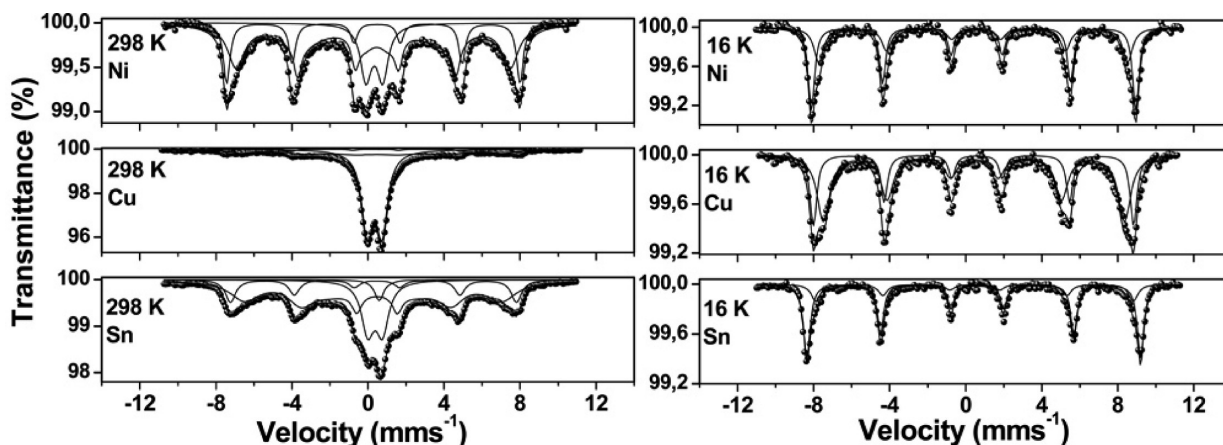
Figure 3. [57]Fe Mössbauer spectra of samples recorded at room temperature (RT) and 16 K. The [119]Sn Mössbauer spectrum of Sn-doped samples is displayed in Figure S1 in the Supporting Information.

the presence of significant magnetic relaxation. The spectra are all fitted to a model considering a discrete sextet corresponding to hematite with structural defects or residual hydroxyl groups within its structure,[18] a hyperfine magnetic field distribution quite broad and asymmetric that likely contains both hematite and maghemite contributions,[10] and a quadrupole doublet due to a fraction of spinel particles with a particle size small enough to show superparamagnetic behavior at RT. In accordance with this picture, the Mössbauer spectra recorded at 16 K (Figure 3, Table S1 in the Supporting Information) are all much narrower and can be fitted to only two discrete components with parameters associated with α-Fe$_2$O$_3$ and γ-Fe$_2$O$_3$ iron oxide polymorphs that are totally blocked at this temperature. The [119]Sn Mössbauer spectrum of the Sn-doped sample (Figure S1 in Supporting Information) only shows the typical singlet corresponding to nonmagnetic Sn^{4+}; that is, the sextet associated with the supertransferred hyperfine interaction with Fe cations is not detected.[16] This result clearly discards the isomorphous substitution of Fe cations by Sn^{4+} cations. A simple association based on the similarity of the [57]Fe Mössbauer spectra of the Sn-, Ni-, and Cu-doped samples at RT and especially at 16 K where unequivocally undoped α-Fe$_2$O$_3$ and γ-Fe$_2$O$_3$ are detected seems to also suggest the absence of isomorphous substitution for the Ni and Cu samples.

From the Mössbauer analysis, we can conclude that at RT (about the operational temperature for MRI applications) the main difference between samples comes from both the relative content maghemite/hematite and the content in superparamagnetic component (maghemite particle size). In fact, a detailed analysis of the contribution to the [57]Fe Mössbauer spectra at RT of both the quadrupole doublet and the signal fitted to a hyperfine magnetic field distribution (Figure 3, Table S1) tells us that the maghemite particle size for the Cu-doped samples is the smallest one (63% for the quadrupole doublet *vs* 21 and 16% for Ni and Sn-samples).

The smallest maghemite particle size is probably a consequence of the much lower temperature needed to obtain the Cu-doped sample (175 °C), and clearly indicates that the role of the Cu (II) doping cations is to promote the formation of γ-Fe$_2$O$_3$ nuclei (iron oxide spinels probably nucleate on surfaces enriched with these cations). The differences between the [57]Fe Mössbauer spectra at RT for Ni and Sn samples are more subtle. Although the relative area of the doublet is slightly lower in Ni than in Sn samples (16 *vs* 21%), the signal fitted to a hyperfine magnetic field distribution is much broader in the Sn-doped sample and both its average and maximum hyperfine magnetic fields are lower. Therefore, despite being obtained at the same temperature (275 °C) the results suggest that, at RT, the Sn-doped sample has a more marked superparamagnetic character than the Ni-doped material. We can, thus, conclude that the crystallite size of maghemite (the phase responsible for enhancing proton relaxivity values) increases from Cu- to Sn- and to Ni-doped samples. This result is particularly important since the magnetic moment of nanosized iron oxide spinels strongly decreases with size and dipolar interactions scale with the radii, r^6. From the analysis of the relative areas at 16 K, we can estimate that the relative content of maghemite with respect to hematite is the highest for the Cu-doped samples (64% γ-Fe$_2$O$_3$ and 36% α-Fe$_2$O$_3$) and smaller in the Ni-doped (36% γ-Fe$_2$O$_3$ and 64% α-Fe$_2$O$_3$) and Sn-doped sample (20% γ-Fe$_2$O$_3$ and 80% α-Fe$_2$O$_3$). Thus, the role of the Ni (II) when compared to Sn (IV) cations is similar, though less intense, to that mentioned for Cu (II) cations (to promote the formation of γ-Fe$_2$O$_3$ nuclei).

Magnetization curves at RT (Figure 4) show that all curves display superparamagnetic-like behavior (zero coercivity field). Ni samples present the highest values of the magnetization at 5 T (13.8 emu/g) while the values for Cu and Sn are 6.0 and 2.0 emu/g, respectively. These values are in the line inferred from Mössbauer spectroscopy and are the result of the simultaneous

contribution of both the content and particle size of maghemite (lowering both causes lower magnetization values). We also present in Figure 4 the results obtained for Mn-doped samples which were prepared in a similar way to that previously reported by some of us, though in this case with a content in Al_2O_3 of 20 instead 10 wt %.[10] Mn-doped samples present a superior magnetization at 5 T (25.8 emu/g) to those containing Ni, Cu, and Sn while still displaying no coercivity. It is also remarkable that the magnetization at 5T was significantly higher when adding 20 wt % of Al_2O_3 instead of the previously reported 10 wt % (26 *vs* 10 emu/g).[10] Zero-field-cooling (ZFC) and field cooling (FC) curves can be used as a simple tool to qualitatively estimate the presence of magnetic dipolar interactions. The temperature dependence of the magnetization **M**(T) taken in FC conditions shows signatures of strong interaction through the observed flattening below the maximum of the ZFC.[19] The curves were registered preserving the alumina coating in the samples to minimize possible interactions between nanorods. Thus, in our system this interaction mainly comes from the γ-Fe_2O_3 clusters encapsulated in the α-Fe_2O_3 matrix.

From the analysis of the FC curve at temperatures higher than the so-called irreversibility temperature (defined as the temperature where the ZFC and FC curves start to diverge), the dipolar interaction can be characterized by a parameter, T^*, proportional to the root mean square (rms) dipolar energy, which appears in the denominator of a modified Langevin function analogous to a Curie−Weiss law.[20] Experimentally, this parameter can be obtained through the expression, $\chi = \mu^2/3k_B(T + T^*)$, where $\chi = 1/$**M** is the susceptibility, μ is the magnetic moment per particle, and k_B is the Boltzmann constant. The analyses have to be restricted to Sn, Cu, and Ni-doped samples since the number of points above the irreversibility temperature for Mn-doped samples is too low to a ensure good statistic. Thus, the values of T^* (so dipolar interaction) increase from 90 to 135 K and 220 K for Sn-, Cu- and Ni-doped samples, respectively. These values suggest that Ni-doped samples will show the highest r_2 values among these samples. Indeed relaxivity measurements carried out in colloidal aqueous suspensions (see Methods for details) of particles having hydrodynamic sizes corresponding to single nanorods confirm this trend. Thus, r_2 values increase from 34 to 78 and 278 Fe mM^{-1} s^{-1} for Sn-, Cu-, and Ni-doped samples, respectively. On the other hand, values of r_1 for Sn-, Cu-, and Ni-doped samples were 1.1, 9.8, and 5.5 Fe mM^{-1} s^{-1}, respectively. The Mn-doped sample shows the highest r_2 value (402 Fe mM^{-1} s^{-1}) in close agreement with its higher value of magnetization (26 *vs* 14, 6, and 2 emu/g for Ni, Cu, and Sn) and the temperature in which the ZFC displays its maximum (280 *vs* 260, 220, 230 K for Ni, Cu, and Sn). Relaxivity, r_1, values for this sample were also relatively low (7.8 Fe mM^{-1} s^{-1}). Values of relaxivity are nor-
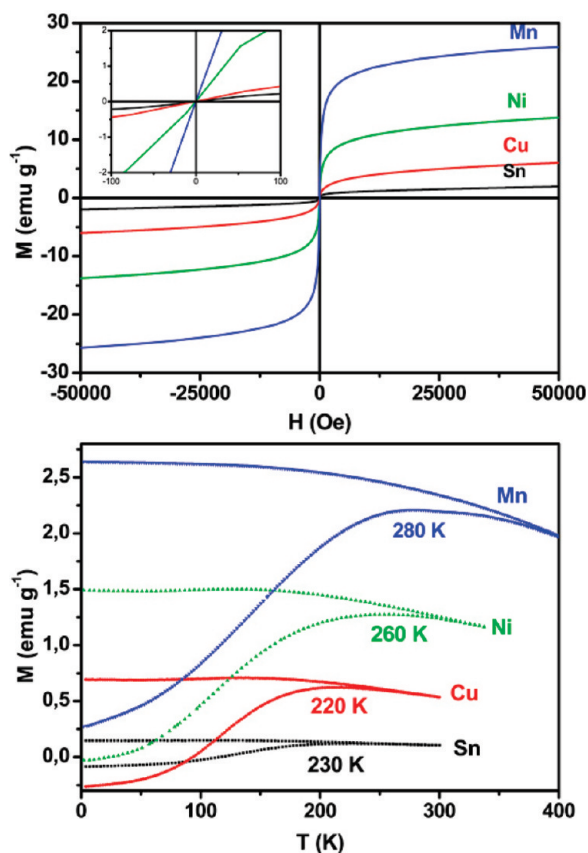

Figure 4. Magnetization curves as a function of applied field (upper graphic) and ZFC/FC curves (lower graphic) of Ni, Cu, and Sn-doped samples. A sample containing Mn is also included. The inset in the magnetization curve shows a zoom at low fields (zero coercivity field, that is, no significant remanence). The values of temperature at which the maxima appear in the ZFC curves are shown.

mally given in Fe concentration since, to our knowledge, in all the reported superparamagnetic contrast agents, all Fe belongs to a magnetically active phase. In our system, however, we have a contribution from a magnetically active phase that induce changes in relaxivity (maghemite) and from an antiferromagnetic phase slightly canted (hematite) whose contribution to changes in relaxivity must be very low. Therefore, to make a reliable comparison of the r_2 values with other systems (especially composites), we have to normalize the results here presented to the content of maghemite. By doing this, we obtain contrast agents with values of r_2 about 800 Fe mM^{-1} s^{-1} (close to the highest reported) while having r_2/r_1 values close to 50 and a magnetic moment of about 25 emu/g. The magnetic moment is an order of magnitude higher than that of aggregates of $MnFe_2O_4$ nanocrystals wrapped first in polymer and then coated with silica-gold nanoparticles (2 emu/g)[6] and almost an order of magnitude lower than that of $Zn_{0.4}Mn_{0.6}Fe_2O_4$ hydrophobic nanoparticles (175 emu/g).[7] Thus, some of the contrast agents here obtained could be, if needed, guided by an external magnetic field while significantly reducing timely
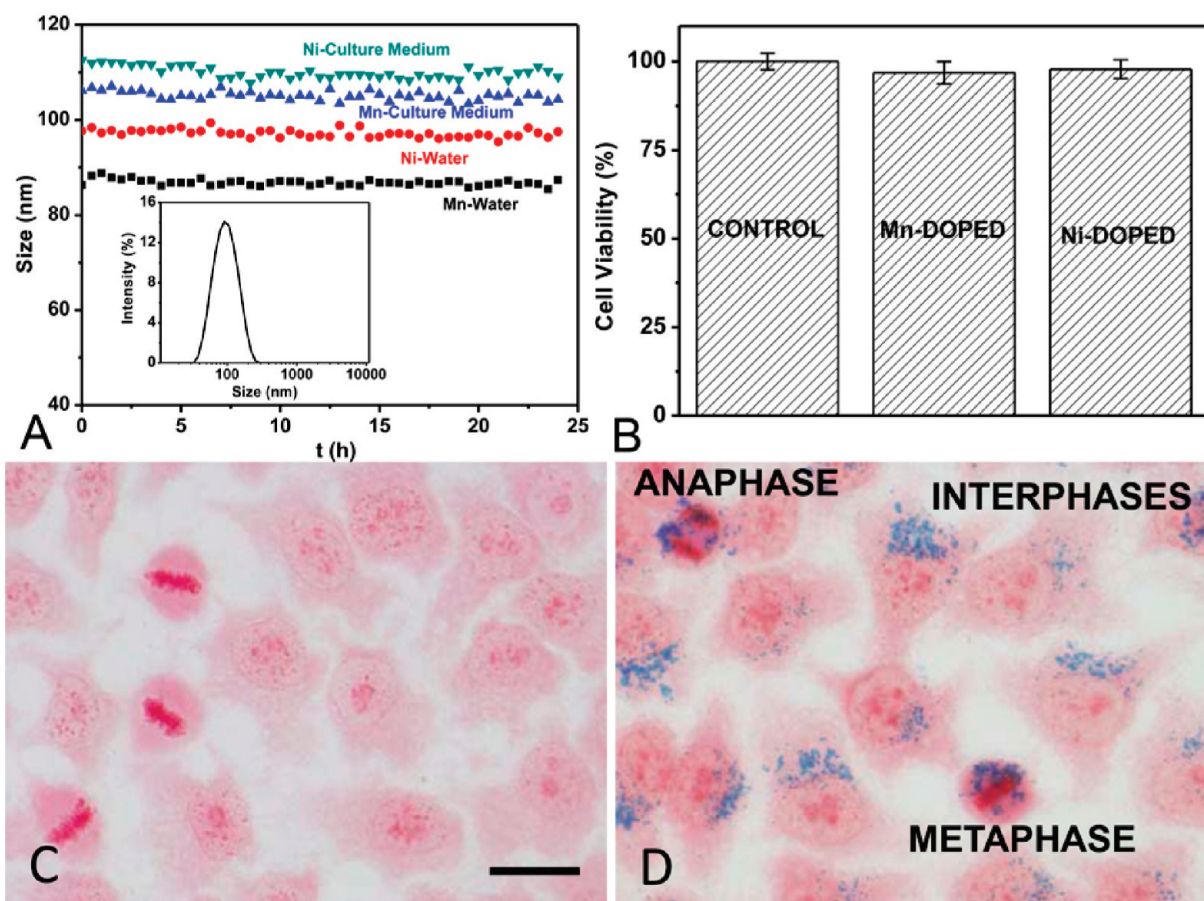
Figure 5. (A) Evolution of the hydrodynamic size as a function of time for the particles showing the highest relaxivity values (Ni- and Mn-doped) dispersed in water and in the same culture medium as the one used for cytotoxicity studies. The inset shows the typical size distribution by intensity of the colloidal dispersions. **(B)** Cytotoxicity studies for the Ni- and Mn-doped samples. Panels C and D are optical micrographs of cells incubated without and with (appear blue, see Methods) nanorods, respectively. The scale bar represents 10 microns. In the micrograph corresponding to the cells incubated with nanorods we can clearly observe cells with nanorods internalized in the cytoplasm. We can also observe cells in different phases of a normal mitosis: cells in the interphase (cell grows accumulating nutrients needed for mitosis), cells in the metaphase (condensed and highly coiled chromosomes align in the middle of the cell before being separated into each of the two daughter), and cells in the anaphase (each chromatid moves to opposite poles of the cell).

driven aggregation induced by high magnetic moments in the highly rich bioenvironments.[21]

Finally, cytotoxicity studies (see Methods for details) were carried out on the colloids showing good contrast agent capabilities (Ni- and Mn-doped samples that have high relaxivity values). Prior to these studies, time-dependent size stability studies (*via* dynamic light scattering, DLS) were carried out on colloidal dispersions of the nanorods in the culture medium used for cell incubation and compared with those obtained in water. The cell culture medium contains proteins, antibiotics, glucose, PBS, aminoacids, fetal bovine serum, *etc.*, and so it provides a biochemically rich environment to test for the colloidal stability of nanorods. Nanorods dispersed in water are stable and present average hydrodynamic sizes that are in the range of the length of the long axis of the nanorods (Figure 5).The same nanorods dispersed in the culture medium are also stable and only a slight increase in the hydrodynamic size probably associated with the interaction with proteins or aminoacids is observed (Figure 5). We should keep in

mind that the measurement of hydrodynamic sizes by DLS is optimized for spherical shape. In our case, we are dealing with elongated particles so the absolute values should be taken cautiously. In any case, it is clear that the hydrodynamic size of the nanorods closely matches the length of their long axis. In addition, the nanorods pass through 0.2 μm pore size membranes. These two results suggest that the size estimated by DLS gives to us a good orientation of the real hydrodynamic size.

Figure 5 also shows that no significant decline in the viability of the HeLa cells was observed in the presence of doped nanorods (no cytotoxicity). Optical micrographs on stained samples (Figure 5) clearly indicate that the nanorods are internalized by the cells (located in the cytoplasm) and that the normal growth of the cells is not altered (see Methods for experimental details). In particular in the optical micrograph corresponding to the cells incubated with nanorods we can clearly observe cells with nanorods internalized (appear as blue stained) in the cytoplasm. We can also observe

cells in different phases of mitosis. Thus, we observe cells in the interphase (cell grows accumulating nutrients needed for mitosis). We can also observe cells in the metaphase (condensed and highly coiled chromosomes, carrying genetic information, align in the middle of the cell before being separated into each of the two daughter), and even cells in the anaphase (each chromatid moves to opposite poles of the cell, the opposite ends of the mitotic spindle, near the microtubule organizing centers).

CONCLUSIONS

We have shown that a new and simple architectonic design that consists of strongly confined superparamagnetic iron oxide nanoparticles embedded in iron oxide porous nanorods can show high relaxivity values and adequate magnetic moments. Furthermore, we have shown that the high values of relaxivities can be qualitatively explained with the help a simple mean field model. Finally, because we are of the opinion that the strength of the design here presented is not only dictated by its present capacity but also by its future capacity, we list some of the steps to follow (not necessarily in this order) in the near future to improve the capabilities of the contrast agent here prepared: (a) decreasing the size of the nanorods; (b) increasing the pore size and accessibility of the porous structure; (c) increasing the amount of doping while simultaneously carrying out cytotoxicity studies; (d) partial coating with noble metals to add extra sensing capacity; (e) applying all the chemistry reported for iron oxides during the last 5 years to enhance functionality and colloidal stability of these particles (say, *e.g.*, coating with an easy to infiltrate porous silica layer).

METHODS

Preparation of Goethite Precursors. Uniform goethite (α-FeOOH) nanorods (80 × 20 nm) were obtained by the aerial oxidation of $FeSO_4$ following a method described earlier.[10] The method essentially consists in the aerial oxidation of $FeSO_4$ aqueous solutions with Na_2CO_3 at 40 °C. ([$FeSO_4$] = 0.075 mol L^{-1}, [Na_2CO_3] = 0.45 mol L^{-1}, air-flow rate = 2 dm^3 min^{-1}, reaction time = 3 h). The method allows the large scale production of uniform nanorods in water at relatively low temperatures (40 °C) and atmospheric pressure.

Cation Coating. A 1 g portion of goethite was ultrasonically dispersed in 0.25 L of water solution at a pH of 11 or 4 depending on the cation to adsorb. A pH of 11 (goethite surface negatively charged) was selected when a cationic polyelectrolyte (poly(diallyldimethylammonium chloride), PDDA) was needed for cation deposition. A pH of 4 (goethite surface positively charged) was selected when a anionic polyelectrolyte (poly(sodium 4-styrenesulfonate), PSS) was needed for cation deposition. Polyelectrolyte layers were restricted to only one layer instead the normally used three or five layers to favor specific adsorption by the goethite substrate on pH zones where repulsive electrostatic interactions were dominant. Polyelectrolyte deposition was performed in magnetically stirred goethite suspensions (4 g L^{-1}) for 30 min at a pH of 11 (PDDA) or 4 (PSS) and then washed three times. The PDDA and PSS concentrations were set to a value of 2 × 10^{-5} and 10^{-3} M, respectively. Experimental evidence of the polyelectrolyte adsorption was achieved by electrophoretic mobility measurements. pH conditions for deposition and the nature of polyelectrolyte (anionic or cationic) were selected according to the solubility diagrams of cations (Supporting Information, Figure S2) and the values of the isoelectric points. A pH of 3 was set as the lower limit to avoid partial dissolution of the goethite nanorods. Thus, for efficient deposition of Ni (II) and Cu (II) species we proceed as follows: $Ni(NO_3)_2 \cdot 6H_2O$ or $Cu(NO_3)_2 \cdot 5H_2O$ was dissolved at a pH of 4 (Supporting Information, Figure S2) in a suspension containing PDDA-goethite nanorods (1 g/L) and the pH was slowly increased up to pH = 12.5 (pH = 10.5 for Cu) and kept at this pH for 1 h to ensure complete precipitation of Ni or Cu oxyhydroxides (Supporting Information, Figure S2). The surface of Ni or Cu oxyhydroxides are negatively charged at pH = 12.5 (pH = 10.5 for Cu) and so PDDA-goethite nanorods induce strong adsorption after full precipitation of the oxyhydroxides onto the nanorods (avoiding possible desorption during the subsequent washing procedure). The solubility of Sn^{4+} is very low (Supporting Information, Figure S2), thus its addition was carried out very slowly under strong magnetic stirring into a suspension containing PSS-goethite nanorods (1 g/L) at a pH of 3 (lower limit to avoid partial dissolution of goethite). Slow addition assures rapid adsorption of the positively charged Sn oxyhydroxides onto the negatively charged PSS-goethite nanorods (isolectric point of Sn oxyhydroxides is about 4−5). After addition, the suspension was kept at pH = 3 under strong stirring for 1 h further to ensure efficient deposition. After deposition all samples were washed several times and dried in an oven at 50 °C.

Alumina Coating. Once depositing the cation onto the surface of the goethite nanorods we proceeded to deposit the alumina layer. For the alumina coating to be effective we needed to start the deposition at a pH of 3 and to have particles with surfaces negatively charged.[10] However, we found that in the case of Ni- and Cu-coated goethites leaching of Ni (II) and Cu (II) species took place at a pH of 3. So prior to the alumina coating, the Ni-, Cu- and also Sn-coated goethite samples were heated at 200 °C for 2 h (during this treatment goethite transforms to hematite). This treatment increases the stability of the coating and avoids leaching. In the case of the Sn samples the heating was carried out only for homogeneity reasons (same treatment to the one carried out for Ni and Cu samples). After this heating, the methodology followed to deposit the alumina coating (20 wt %) was similar to that previously carried out for alumina (10 wt %)-coated goethite nanorods,[10] though in this case it was carried out for hematite nanorods. Thus, 1 g of Ni-hematite, Sn-hematite, or Cu-hematite nanorods was dispersed in 1 L of an aqueous solution. The dispersion was brought to a pH of 4 (3 for the Sn samples) and kept in ultrasound for 1 h. Polyelectrolyte deposition was performed in magnetically stirred nanorod suspensions (1 g L^{-1}) for 30 min at a pH of 4 (3 for the Sn samples), where the surface of the nanorods is positively charged and the anionic polyelectrolyte (PSS) can be easily adsorbed. The PSS concentration was set to a value of 10^{-3} M. Experimental evidence of the polyelectrolyte adsorption was achieved by electrophoretic mobility measurements. After washing, the negatively charged PSS-nanorods were ultrasonically dispersed for 1 h at a pH of 3, and then the necessary amount of $Al(NO_3)_3$ (20 mol %) was added to the dispersion. Then the magnetically stirred dispersion was slowly titrated with KOH 0.5 M up to a pH of 6.5 (30 min of titration). The dispersion was kept at a pH of 6.5 for 1 h (using KOH 0.5 M) and then was brought to pH 7.5 (using KOH 0.5 M). At this pH the dispersion was kept 1 h longer to ensure complete precipitation. By using this methodology we ensure the complete precipitation of the positively charged Al oxyhydroxide compounds onto the negatively charged PSS-cation-hematite nanorods. At pH values of 6.5 and 7.5 the Al oxyhydroxide compounds are positively charged.

Thermal Treatment and Reduction. Prior to reduction all the samples were thermally treated in air at 200 °C for 2 h. Sn and Ni samples were reduced at 275 °C in a H_2 stream of 20 L h^{-1} for 2 h (for Cu the temperature of reduction was 175 °C). The

samples were then cooled to room temperature under the hydrogen atmosphere. Finally, nitrogen gas was blown into a flask containing ethanol, and the resulting stream was passed through the sample (~1 h) to avoid rapid corrosion in case the reduction led to metallic iron (it turned out that under these relative low temperatures no metallic iron can be developed).

Colloidal Stabilization of Suspensions for Relaxivity Measurements. To show that contrast agents based on superparamagnetic clusters of γ-Fe_2O_3 nanoparticles embedded in α-Fe_2O_3 porous nanorods have high relaxivities, we prepared stable colloidal suspensions containing the nanorods. First, the alumina coating was removed by stirring the suspensions at a pH of 14 during 24 h. Then, the following protocol was used to graft carboxylates to the surface of particles: 2.5 mL of HNO_3 (1 M) were added to 0.5 g of sample (referred to the Fe content), and the resulting suspension was ultrasonically treated for 30 min followed by heating at 80 °C during 30 min in an oven using capped tubes. Then, 10 g of citric acid was added to the mixture, and again the mixture was ultrasonically treated for 30 min and heated at 80 °C during 30 min in an oven using capped tubes. Subsequently, we added 15 mL of water, and the resulting suspension was again ultrasonically treated for 30 min and heated at 80 °C during 30 min in an oven using closed tubes. Finally, the suspension was centrifuged twice (first time at 6000 rpm and second time at 12000 rpm), dispersed in 100 mL of water (final concentration, 5 mg of Fe/mL) and kept until further use at 4 °C. Prior to their use in different studies the samples were ultrasonically treated for 1 h.

Crystallochemical Characterization. The diffraction pattern (XRD) was obtained on Bruker AXS instrument operating at 40 KV and 30 mA, using Cu Kα radiation (λ = 0.15406 nm). The particles size and shape were examined by tomography emission microscopy, TEM (JEOL 2000 FX). The high-resolution tomography emission microscopy, HRTEM image was obtained on a 300 kV JEOL-3000 instrument. The cation content in the goethite/hematite acicular matrix was determined by plasma emission, ICP (Perkin-Elmer 5500). Chemical analyses of samples at the single particles level was accomplished using an EDX analyzer (Oxford link QX 2000), integrated in the TEM. Magnetic properties at room temperature were recorded using a vibrating sample magnetometer (MLVSM9Maglab 9T, Oxford Instruments). The temperature dependence of the magnetization was monitored by zero- field cooling (ZFC) and field cooling (FC) experiments. The ZFC curve was obtained by first cooling the system in a zero magnetic field to 5 K. Then a magnetic field was applied (50 Oe), and the magnetization was measured while the temperature was increased. The FC curve was obtained in a similar way except that the sample was cooled in the measuring field (50 Oe). Transmission ^{57}Fe Mössbauer spectra were recorded using a conventional constant-acceleration spectrometer equipped with a ^{57}Co (Rh) source. The absorbers were prepared to yield an effective thickness of about 10 mg cm^{-2} of natural Fe. In some cases, low temperature spectra (16 K) were recorded using a closed-cycle He cryogenerator Air Products. All the spectra were computer-fitted to obtain the peak position and areas. Isomer shifts were referred to the centroid of the spectrum of α-Fe at room temperature. The ^{119}Sn Mössbauer spectra were recorded at RT using a ^{119}Sn source, and the tin isomer shifts were referred to SnO_2.

Colloidal Characterization and Relaxivities Measurements. Measurements of the electrophoretic mobility and hydrodynamic sizes were carried out using a Zetasizer Nano instrument from Malvern Instruments. Relaxivities r_1 and r_2 (60 MHz) were measured at 1.41 T with a Minispec Mq-60 Bruker spectrometer. The nanorods were dispersed in water at different Fe concentrations (0–1 mM). The efficiency of an MRI contrast agent is commonly assessed in terms of its relaxivities r_1 and r_2, which are rates of proton relaxation and are determined according to the equation $1/T_{i,obs} = 1/T_{i,d} + r_i$ [M] (i = 1, 2) where $1/T_{i,obs}$ is the observed solvent relaxation rate in the presence of a contrast agent, $1/T_{i,d}$ is the relaxation rate of the pure diamagnetic solvent, and [M] is the concentration of the contrast agent. T_1 measurements were obtained using the standard inversion–recovery pulse sequence, which consists in an inversion (180°) pulse followed by a 90° reading pulse. The measurement of T_1 consisted thus in re-

peating this sequence several times, each sequence being separated from the next one by the recovery delay ($5T_1$). T_2 measurements were obtained using the Carr–Purcell–Meiboom–Gill pulse sequence. In this sequence, a 90° pulse is followed by a series of 180° pulses, covering the full decay of the signal. The recovery delay between sequences was again set to $5T_1$.

Cell Culture, Viability of Cells (Cytotoxicity Studies), and Nanorods Internalization in the Cells. HeLa (human cervical carcinoma) cells were grown as monolayers in Dulbecco's modified Eagles's medium (DMEM) with 50 units ml^{-1} penicillin and 50 μg mL^{-1} streptomycin and supplemented with fetal bovine serum (FBS), at a final concentration of 10%. All the media, sera, and antibiotics were provided by Gibco (Paisley, U.K.). Cell cultures were performed in a 5% CO_2 atmosphere at 37 °C and maintained in an incubator. For the experiments, the cells were seeded into 24 multiwell plates at an initial density of 3500 cells/well. Treatments were initiated 3 days after plating (approximately 70% confluence). Depending on the experiments, the cells were seeded on 10 mm square glass coverslips placed into the wells. To analyze the internalization of nanoparticles, HeLa cells were grown on coverslips and incubated for 1–24 h (0.5 mg Fe ml^{-1} culture medium). The viability of HeLa cells (cytotoxicity studies) was determined using a standard methyl thiazol tetrazolium bromide (MTT) assay (Sigma, St Louis, MO). Briefly, 24 h after incubation with nanoparticles, MTT was added to each well (the final concentration of MTT in medium was 50 μg mL^{-1}) for 3 h at 37 °C. The formazan that formed in the cells was dissolved adding 0.5 mL of DMSO in each dish, and the optical density was evaluated at 570 nm in a microplate reader (Tecan Spectra Fluor spectrophotometer). Cell survival was expressed as the percentage of absorption of treated cells in comparison with that of control cells (not nanoparticles present during incubation). The results obtained are the mean value and standard deviation (SD) from at least six experiments. To determine the location of nanorods, the cells preincubated with the nanorods were stained with Prussian blue (sensitive to iron). Thus, the cells were fixed in ice-cold methanol (5 min), stained with an equal volume of 1 N hydrochloric acid and 10% potassium ferrocyanide trihydrate for 1 h, and counterstained with 1% neutral red for 3 min. The preparations were then washed with distilled water, air-dried, and mounted in DePeX (Serva, Germany). Optical micrographs of these preparations were taken with an Olympus BX61 under bright light illumination.

Time-Dependent Size Stability Studies of the Nanorods in a Biochemically Rich Environment (*via* Dynamic Light Scattering). The culture medium used for HeLa cells growth was also used for time-dependent size stability studies of the nanorods in a biochemically rich environment (*via* dynamic light scattering using a Zetasizer Nano Instrument from Malvern Instruments).

Supporting Information Available: Table S1 with Mössbauer data, Figure S1 with the ^{119}Sn Mössbauer, and Figure S2 with solubility diagrams. This material is available free of charge *via* the Internet at http://pubs.acs.org.

REFERENCES AND NOTES

1. Lauffer, R. E. Paramagnetic Metal Complexes as Water Proton Relaxation Agents for NMR Imaging: Theory and Design. *Chem. Rev.* **1987**, *87*, 901.
2. Mornet, S.; Vasseur, S.; Grasset, F.; Duguet, E. Magnetic Nanoparticle Design for Medical Diagnosis and Therapy. *J. Mater. Chem.* **2004**, *14*, 2161.
3. Laurent, S.; Forge, D.; Port, M.; Roch, A.; Robic, C.; Elst, L. V.; Muller, R. N. Magnetic Iron Oxide Nanoparticles: Synthesis, Stabilization, Vectorization, Physicochemical Characterizations, and Biological Applications. *Chem. Rev.* **2008**, *108*, 2064.
4. Mendonca, M. H.; Lauterbur, P. C. Ferromagnetic Particles as Contrast Agents for Magnetic Resonance Imaging of Liver and Spleen. *Magn. Reson. Imaging* **1986**, *3*, 328.

5. Ai, H.; Flask, C.; Weinberg, B.; Shuai, X.; Pagel, M. D.; Farrell, D.; Duerk, J.; Gao, J. Magnetic-Loaded Polymeric Micelles as Ultrasensitive Magnetic-Resonance Probes. *Adv. Mater.* **2005**, *17*, 1949.

6. Lee, J.; Yang, J.; Ko, H.; Oh, S. J.; Kang, J.; Son, J.-H.; Lee, K.; Lee, S.-W.; Yoon, H.-G.; Suh, J.-S.; Huh, Y.-M.; Haam, S. Multifunctional Magnetic Gold Nanocomposites: Human Epithelial Cancer Detection *via* Magnetic Resonance Imaging and Localized Synchronous Therapy. *Adv. Funct. Mater.* **2008**, *18*, 258.

7. Jang, J.-T.; Nah, H.; Lee, J.-H.; Moon, S. H.; Kim, M. G.; Cheon, J. Critical Enhancements of MRI Contrast and Hyperthermic Effects by Dopant-Controlled Magnetic Nanoparticles. *Angew. Chem., Int. Ed.* **2009**, *48*, 1234.

8. Rebolledo, A. F.; Fuertes, A. B.; Gonzalez-Carreno, T.; Sevilla, M.; Valdes-Solis, T.; Tartaj, P. Signatures of Clustering in Superparamagnetic Colloidal Nanocomposites of an Inorganic and Hybrid Nature. *Small* **2008**, *4*, 254.

9. Lopez, C. Materials Aspects of Photonic Crystals. *Adv. Mater.* **2003**, *15*, 1679.

10. Rebolledo, A. F.; Bomatí-Miguel, O.; Marco, J. F.; Tartaj, P. A Facile Synthetic Route for the Preparation of Superparamagnetic Iron Oxide Nanorods and Nanorices with Tunable Surface Functionality. *Adv. Mater.* **2008**, *20*, 1760.

11. Chithrani, B. D.; Ghazani, A. A; Chan, W. C. W. Determining the Size and Shape Dependence of Gold Nanoparticle Uptake into Mammalian Cells. *Nano Lett.* **2006**, *6*, 662.

12. Caruso, F. Nanoengineering of Particle Surfaces. *Adv. Mater.* **2001**, *13*, 11.

13. Madden, A. S.; Hochella, M. F. A., Jr. A Test of Geochemical Reactivity as a Function of Mineral Size: Manganese Oxidation Promoted by Hematite Nanoparticles. *Geochim. Cosmochim. Acta* **2005**, *69*, 389.

14. Cross, W. B.; Affleck, L.; Kuznetsov, M. V.; Parkin, I. P; Pankhurst, Q. A. Self-Propagating High-Temperature Synthesis of Ferrites MFe_2O_4 (M = Mg, Ba, Co, Ni, Cu, Zn); Reactions in an External Magnetic Field. *J. Mater. Chem.* **1999**, *9*, 2545.

15. Zuo, X.; Aria, Y.; Vittoria, C; Harris, V. G. Computational Study of Copper Ferrite ($CuFe_2O_4$). *J. Appl. Phys.* **2006**, *99*, 08M909.

16. Berry, F. J.; Bohorquez, A.; Helgason, O.; Jiang, J. Z.; McManus, J. G.; Moore, E.; Mortimer, M.; Mosselmans, F.; Morup, S. An Investigation of the Local Environments of Tin in Tin-Doped α-Fe_2O_3. *J. Phys.: Condens. Matter.* **2000**, *12*, 4043.

17. Song, Q.; Zhang, Z. J. Correlation between Spin-Orbital Coupling and the Superparamagnetic Properties in Magnetite and Cobalt Ferrite Spinel Nanocrystals. *J. Phys. Chem. B* **2006**, *110*, 11205.

18. Murad, E.; Johnston, J. H. Mössbauer Spectroscopy Applied to Inorganic Chemistry,Long, G. J., Ed.; Plenum: New York/London, 1987; p 507.

19. Knobel, M.; Nunes, W. C.; Socolovsky, L. M.; De Biasi, E.; Vargas, J. M.; Denardin, J. C. Superparamagnetism and Other Magnetic Features in Granular Materials: A Review on Ideal and Real Systems. *J. Nanosci. Nanotechnol.* **2008**, *8*, 2836.

20. Allia, P.; Coisson, M.; Tiberto, P.; Vinai, F.; Knobel, M.; Novak, M. A.; Nunes, W. C. Granular Cu−Co Alloys as Interacting Superparamagnets. *Phys. Rev. B* **2001**, *64*, 144420.

21. Tartaj, P. Superparamagnetic Composites: Magnetism with No Memory. *Eur. J. Inorg. Chem.* **2009**, 333.

ARTICLE